A nonlinear theory for multidimensional relativistic plasma wave wakefields[a)]

W. Lu,[b)] C. Huang, M. Zhou, and M. Tzoufras
Department of Electrical Engineering, UCLA, Los Angeles, California 90095

F. S. Tsung
Department of Physics and Astronomy, UCLA, Los Angeles, California 90095

W. B. Mori
Department of Electrical Engineering and Department of Physics and Astronomy, UCLA, Los Angeles, California 90095

T. Katsouleas
Department of Electrical Engineering, USC, Los Angeles, California 90089

(Received 8 November 2005; accepted 12 April 2006; published online 26 May 2006)

A nonlinear kinetic theory for multidimensional plasma wave wakes with phase velocities near the speed of light is presented. This theory is appropriate for describing plasma wakes excited in the so-called blowout regime by either electron beams or laser pulses where the plasma electrons move predominantly in the transverse direction. The theory assumes that all electrons within a blowout radius are completely expelled. These radially expelled electrons form a narrow sheath just beyond the blowout radius which is surrounded by a region which responds weakly (linearly). This assumption is reasonable when the spot size of the electron beam and laser are substantially less than the blowout radius. By using this theory one can predict the wakefield amplitudes and blowout radius in terms of the electron beam or laser beam parameters, as well as predict the nonlinear modifications to the wake's wavelength and wave form. For the laser case, the laser spot size must also be properly matched in order for a narrow sheath to form. The requirements for forming a spherical wave form, i.e., "bubble," are also discussed. The theory is also used to show when linear fluid theory breaks down and how this leads to a saturation of the logarithmic divergence in the linear Green's function. © *2006 American Institute of Physics*. [DOI: 10.1063/1.2203364]

I. INTRODUCTION

The theory of one-dimensional (1D), nonlinear plasma oscillations in cold plasmas has a long history beginning with the pioneering work of Ahkiezer and Polovin,[1] and Dawson.[2] Ahkiezer and Polovin studied purely one-dimensional longitudinal and transverse oscillations in cold plasmas including relativistic mass effects. In the work of Dawson, nonrelativistic treatments of purely 1D longitudinal oscillations were studied, including radial and spherical oscillations. He showed that trajectory crossing occurs in either radial or spherical oscillations even for arbitrarily small amplitudes. However, more than 40 years later there is still no theory for multidimensional [two or three dimensional (2D/3D)], nonlinear plasma oscillations associated with waves with phase velocities near the speed of light, c. Such oscillations are complicated because the fields are electromagnetic, relativistic mass effects are important, and trajectory crossing occurs. Besides being of great fundamental interest, a class of these nonlinear multidimensional plasma waves are of great importance to plasma-based acceleration.

In plasma-based acceleration, a plasma wave with a phase velocity close to the speed of light is driven by an intense particle or laser beam. When a laser beam is used it is called laser wakefield acceleration (LWFA) (Ref. 3), and when a particle beam is used it is called plasma wakefield acceleration (PWFA) (Ref. 4). Most theories to date on wakefield excitation have either been restricted to linear fluid theory[4,5] or one-dimensional nonlinear fluid theory.[1] However, in recent PWFA and LWFA experiments[6,7] the wakes are excited in the so-called blowout regime where neither fluid nor one-dimensional theory applies. In the blowout regime, the wake is excited by the space charge of the beam or the radiation pressure of the laser expelling plasma electrons radially outward leaving behind a "channel" of unshielded ions. These expelled, blown-out, electrons form a narrow sheath just outside the ion channel. Eventually the space charge of the ions pulls the electrons back, thereby creating the plasma wave wake. This is illustrated in Fig. 1, where the electron density is plotted from a fully nonlinear particle-in-cell (PIC) simulation using the code OSIRIS (Ref. 8). The electron beam is propagating to the left in the variable $\xi = ct - z$. The blowout or ion channel radius, r_b, is also defined in this plot. This figure makes clear that the radius of the channel is not constant, i.e., it depends on $\xi = ct - z$.

The blowout regime of creating wakefields was first investigated by Rosenzweig *et al.*[9] for electron beam drivers. They pointed out that these wakefields had perfectly linear focusing fields and had an acceleration gradient that was

[a)]Paper FI2 3, Bull. Am. Phys. Soc. **50**, 105 (2005).
[b)]Invited speaker.

 © 2006 American Institute of Physics

Downloaded 06 Jun 2006 to 198.11.27.24. Redistribution subject to AIP license or copyright, see http://pop.aip.org/pop/copyright.jsp

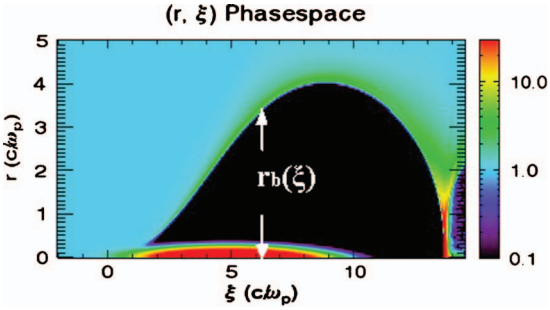

FIG. 1. (Color) Electron charge density with the defined blowout radius $r_b(\xi)$.

constant in radius for electrons. For sufficiently intense drivers the ion channel can have a spherical, i.e., bubble, shape. Therefore, in some of the recent work on LWFA the term bubble[10] is used. Despite this intense interest, there is little theory for how the wakefields in the blowout regime scale with the electron beam or laser beam parameters, and no theory exists for how beam loading occurs within these nonlinear multidimensional wakes. In addition, while there are expressions for the nonlinear frequency shift[1] for one-dimensional wakes there is no such expression for multidimensional wakes.

The blowout regime also has relevance to the linear theory of wake excitation. It is well known that the Green's function of a relativistically moving point particle logarithmically diverges with the inverse of the radial position behind the particle. It had been argued rather nonrigorously that this divergence breaks down for r less than the Debye length[4] or the Compton wavelength.[11] In a cold plasma the Debye length is zero and since the theory is classical one should attempt to obtain a physical reason within the scope of classical theory. Simulations have shown that the wakes made by narrow bunches do indeed saturate for r smaller than a critical value.[5] The present work provides a clear explanation as to why this occurs and, therefore, when and why fluid theory breaks down. For any amount of charge one can shrink the beam's spot size down to a value for which blowout occurs. The linear Green's function is not valid for radii within the region void of electrons. For small blowout radius the influence of the electrons within and beyond the sheath becomes very important while within the blowout radius one needs a different description of plasma oscillations which this new theory provides.

Recently, Barov *et al.*,[12] Lotov,[13] and Kostyukov *et al.*[14] each theoretically analyzed the limit of large blowout radius (Lotov calls it the "cavern" while Kostyukov calls it the "bubble" regime). Barov treated the energy loss of an infinitesimally short electron beam. Lotov provided a qualitative analysis of the blowout regime for the PWFA, but his main results differ profoundly from ours. For example, he obtains the scaling between the blowout radius and the axial length L_c of the ion channel ("cavern") $k_p L_c \propto k_p^3 r_m^3$ for large $k_p r_m$, where r_m is the maximal blowout radius; while we will show later that when $k_p r_m \gtrsim 4$, the ion channel is a sphere, i.e., $L_c = r_m$. Kostyukov observed in simulations that for laser drivers the ion channel is indeed a sphere ("bubble") and derived the field structure for such shapes moving at the speed of light. Very recently, Gordienko and Puhkov[15] presented a similarity theory for wakefield acceleration driven by laser drivers. This theory provides a mechanism for scaling results from one simulation or experiment to others provided that the laser profile remains the same; that the relevant laser, space, and time variables are scaled properly; and that the laser intensity is very high. However, these analyses neither explain why there is a bubble, nor can they predict the field structure in wakes created by beam drivers or weaker lasers.

In this paper, we will present a predictive theoretical model for wake excitation by particle beam or laser drivers that are narrow enough to excite the wake in the blowout regime. The spot size must be less than the blowout radius and this is quantified in terms of the electron or laser beam parameters later. This theory can be used to understand the limitations of the cold fluid theory and to explore the blowout regime for either laser or particle beam drivers. The theory is valid for arbitrary blowout radius making it possible to understand why the ion column is roughly spherical for large blowout radius. The theory can also be used to develop a theory for electron hosing, for nonlinear beam loading, and for pulse shaping. The key idea behind the theory is that the wake can be described entirely in terms of the trajectory of the blowout radius, $r_b(\xi)$. This can be done because the blown-out electrons form a sheath whose thickness is narrower than the blowout radius, even for small values of r_b. This key assumption does not always hold for laser drivers. The paper is outlined as follows. In Sec. II the basic equations are described. In Sec. III the condition for sheet crossing is given. In Sec. IV an equation for the blowout radius is derived. In Secs. V and VI the limits of small and large blowout radius are considered, respectively. In Sec. VII formulas for arbitrary blowout radius are derived. In Sec. VIII the differences between using a laser versus a particle beam driver are described, and the work is summarized in Sec. IX.

II. THE BASIC EQUATIONS FOR WAKE EXCITATION

In a theoretical description of short laser pulses or ultrarelativistic charged particle beams interacting with underdense plasmas, one needs to self-consistently treat both the electromagnetic fields and the trajectories for the plasma particles. For the electromagnetic fields, the full set of Maxwell's equations or some reduced form can be used and due to their linear origin, once the currents and charge densities are known, they can be easily solved subject to appropriate boundary conditions (including no boundary at all). Therefore, the nonlinearities and complexities come from the description of plasma. Indeed this is true for all kinds of nonlinear laser-matter interactions. The simplest model for a plasma is a cold fluid model, which is valid for describing laser or beam plasma interactions as long as the particle trajectories do not cross. Unfortunately, particle trajectory crossing is so pervasive in laser plasma or beam plasma interactions that except for linear or weakly nonlinear cases,

Downloaded 06 Jun 2006 to 198.11.27.24. Redistribution subject to AIP license or copyright, see http://pop.aip.org/pop/copyright.jsp

the single cold fluid model always breaks down. This situation is painfully evident when multidimensional oscillations are considered.

In 1959, Dawson already pointed out that trajectory crossing will happen after a period of time for purely radial or spherical cold plasma oscillations, as long as very weak nonlinearities are taken into account. The reason for this is that the nonlinearities will induce initial position-dependent frequency shifts, which eventually cause particles to oscillate out of phase with each other leading to trajectory crossing. Interestingly, 1D planar nonrelativistic oscillations lack this kind of phase mixing due to the fact that there is no frequency shift for this case. As a result, particle crossing in 1D planar oscillations only occurs for rather large oscillation amplitudes, e.g., the 1D wavebreaking limit. As Dawson showed, this is also the condition when some particles get trapped in the wave, i.e., their velocity exceeds the phase velocity of the wave. This special property for the 1D planar case leads to a confusing use of the words "wavebreaking" and "trapping" in the literature. The original meaning of "wavebreaking" in Dawson's classic paper is closer to "trajectory crossing" than "trapping." As we just discussed, in one dimension they always happen together; however, for nonplanar oscillations, "trajectory crossing" can happen very easily for even very small amplitude without particles getting "trapped." We will adopt the term "trajectory crossing" as the meaning of "wavebreaking" to emphasize the breakdown of a single cold fluid model.

In light of Dawson's work, we can see that even for very weakly nonlinear multidimensional laser plasma or beam plasma interactions the cold fluid model can only be valid for a finite time or alternatively for a finite region in space. For example, in the cases of weak and short drivers (by weak, we only mean that the density perturbation caused by the driver is small compared with the ambient plasma density), for the region not too far behind the driver, the fluid model is valid. This region could be many plasma wavelengths long for a weak driver. On the contrary, if the trajectory crossing happens near the driver, the fluid model breaks down totally and a model which includes the blowout regime is essential in this case. For a particle beam driver, one does not necessarily need a strong driver in order to cause blowout.

From this discussion, it is clear that a particle picture must be used for a general treatment of the laser or beam plasma interaction. This is equivalent to a multispecies cold fluid model where particles within each species execute cold laminar flow without trajectory crossing.

To analyze general multidimensional plasma oscillations excited by an intense particle beam or laser beam, we therefore start from Maxwell's equations in the Lorentz gauge and the equation of motion for an arbitrary number of laminar fluids,

$$\left(\frac{1}{c^2}\frac{\partial^2}{\partial t^2}-\nabla^2\right)\begin{bmatrix}\boldsymbol{A}\\ \phi\end{bmatrix}=4\pi\begin{bmatrix}\boldsymbol{J}/c\\ \rho\end{bmatrix}, \tag{1}$$

$$\frac{1}{c}\frac{\partial\phi}{\partial t}+\boldsymbol{\nabla}\cdot\boldsymbol{A}=0, \tag{2}$$

$$\left(\frac{\partial}{\partial t}+\boldsymbol{V}_i\cdot\nabla\right)\boldsymbol{P}_i=q_i\left[\boldsymbol{E}+\frac{\boldsymbol{V}_i}{c}\times\boldsymbol{B}\right], \tag{3}$$

where $\rho=\Sigma_i q_i n_i$, $\boldsymbol{J}=\Sigma_i q_i n_i \boldsymbol{V}_i$, they satisfy the charge conservation equation

$$\frac{\partial\rho}{\partial t}+\nabla\cdot\boldsymbol{J}=0. \tag{4}$$

We next make several simplifications: The first one is that upstream from the laser or beam driver, each fluid can be treated as at rest or cold. For tenuous plasmas, the phase velocity of the excited wakefields is roughly the speed of light, c. Compared with this speed, all the initial thermal velocities of plasma particles can be treated as zero. The second approximation is the wavelike assumption that fields in the wake depend on the variable $\xi\equiv(ct-z)$, where the phase velocity of the wave is essentially c. The last approximation is called the "quasistatic approximation"[16] or "frozen field approximation,"[17] which is based on the multi-time-scale nature of the physical process. The driver evolves on a time scale much longer than the plasma response, so during the time it takes for a driver to pass by a plasma particle, the driver changes shape very little. This suggests that we can take the driver as nonevolving when calculating the plasma response. Therefore, the wake depends weakly on the distance the driver has moved into the plasma.

For this last approximation to be valid, we need different conditions for laser drivers and beam drivers. For the laser case, the driver evolves on a scale length roughly given by the Rayleigh length ($Z_R=\pi W_0^2/\lambda_0$). The laser spot size W_0 is on the order of plasma skin depth c/ω_p, so the quasistatic approximation is valid as long as $\omega_0/\omega_p\gg 1$. For the electron beam case, the driver evolves on a length scale roughly given by the Betatron wavelength, which is $2\pi\sqrt{2\gamma}c/\omega_p$ for a beam particle in an ion channel, so the quasistatic approximation is valid for a beam driver if $\gamma\gg 1$.

It is also worth noting that for extremely strong drivers, some plasma particles are pushed forward in front of the driver with very high parallel velocity, so it takes a rather long time for the driver to pass by these particles. For these particles, the "quasistatic approximation" will fail.

For the laser-driven case there are three time scales: the high-frequency laser oscillation ω_0^{-1}, the plasma wakefield oscillation ω_p^{-1}, and laser envelope evolution $\omega_0/\omega_p\omega_p^{-1}$. When calculating the wakefield excitation only the smooth motion is relevant. This smooth motion can be described by averaging out the high-frequency laser oscillation from the equation of motion. The resulting smooth force from the laser is the ponderomotive force.

$$\frac{d}{dt}\boldsymbol{P}_{is}=\left(\frac{\partial}{\partial t}+\boldsymbol{V}_{is}\cdot\nabla\right)\boldsymbol{P}_{is}=q_i\left[\boldsymbol{E}_s+\frac{\boldsymbol{V}_{is}}{c}\times\boldsymbol{B}_s\right]+\boldsymbol{F}_p. \tag{5}$$

In this equation, the fields $\boldsymbol{E}_s$ and $\boldsymbol{B}_s$ are the smooth fields produced by beam driver and plasma charge density and current. F_p is ponderomotive force of the laser,

Downloaded 06 Jun 2006 to 198.11.27.24. Redistribution subject to AIP license or copyright, see http://pop.aip.org/pop/copyright.jsp

$$\boldsymbol{F}_p = -\frac{q_i^2}{\bar{\gamma}_i m_i c^2}\nabla\left|\frac{\hat{A}_L}{2}\right|^2, \tag{6}$$

where the laser field is written as $A_{\text{laser}}=\hat{A}_L/2e^{-i\omega_0/c\xi}+\text{c.c.}$, $e\hat{A}_L/mc^2\equiv a$, and $\bar{\gamma}_i=(1+P_i^2/m^2c^2+|a|^2/2)^{1/2}$. A thorough derivation was performed by Mora and Antonsen.[18]

At this point, we will adopt normalized units, where time is normalized to ω_p^{-1}, length to c/ω_p, velocities to the speed of light, c, mass to electron mass, m, and charge to electron charge, e; fields to $mc\omega_p/e$, potentials to mc^2/e, charge density to en_p, and current density to en_pc. For convenience, we also omit the subscripts "i" and "s."

To best utilize the quasistatic approximation, we can do a transformation from the (x,y,z,t) variables to the $(x,y,\xi\equiv ct-z,s\equiv t)$. In this group of new variables the quasistatic approximation implies $\partial_s \ll \partial_\xi$ in the field equation. Maxwell's equations then become

$$-\nabla_\perp^2\begin{bmatrix}\boldsymbol{A}\\ \phi\end{bmatrix}=\begin{bmatrix}\boldsymbol{J}\\ \rho\end{bmatrix}, \tag{7}$$

$$\boldsymbol{\nabla}_\perp\cdot\boldsymbol{A}_\perp=-\frac{\partial\psi}{\partial\xi}, \tag{8}$$

where $\psi\equiv\phi-A_z$, $\boldsymbol{\nabla}_\perp\equiv\hat{x}\partial/\partial x+\hat{y}\partial/\partial y$, $\boldsymbol{A}_\perp=\hat{x}A_x+\hat{y}A_y$, etc. Furthermore, it can be shown that the plasma electrons evolve as[18]

$$\frac{d}{d\xi}\boldsymbol{P}_\perp=\frac{1}{1-v_z}\left[-[\boldsymbol{E}_\perp+(\boldsymbol{V}\times\boldsymbol{B})_\perp]-\frac{1}{\bar{\gamma}}\boldsymbol{\nabla}_\perp\frac{|a|^2}{4}\right], \tag{9}$$

where $\bar{\gamma}=(1+P^2+|a|^2/2)^{1/2}$. There is an Eq. (9) for each laminar fluid or Lagrangian fluid particle. It can also be shown that $\bar{\gamma}-P_z=1+\psi$ is a constant of the motion. In this equation all high-frequency motion associated with the laser has been averaged out. As a consequence of the constant of the motion, we can write

$$P_z=\frac{\left[1+P_\perp^2+\dfrac{|a|^2}{2}-(1+\psi)^2\right]}{2(1+\psi)}, \tag{10}$$

$$\bar{\gamma}=\frac{\left[1+P_\perp^2+\dfrac{|a|^2}{2}+(1+\psi)^2\right]}{2(1+\psi)}, \tag{11}$$

$$1-v_z=\frac{2(1+\psi)^2}{\left[1+P_\perp^2+\dfrac{|a|^2}{2}+(1+\psi)^2\right]}, \tag{12}$$

so that once $P_\perp$ is solved, the axial momentum is known. In addition, the pseudopotential ψ obeys the Poisson-like equation,

$$-\nabla_\perp^2\psi=(\rho-J_z), \tag{13}$$

the continuity equation of electric charge becomes

$$\frac{\partial}{\partial\xi}(\rho-J_z)+\nabla_\perp\cdot\boldsymbol{J}_\perp=0, \tag{14}$$

and the fields E_z, B_z, $\boldsymbol{E}_\perp$, and $\boldsymbol{B}_\perp$ can be calculated via

$$E_z=\frac{\partial\psi}{\partial\xi}, \tag{15}$$

$$B_z=(\nabla_\perp\times\boldsymbol{A}_\perp)\cdot\hat{z}, \tag{16}$$

$$\boldsymbol{E}_\perp=-\nabla_\perp\phi-\frac{\partial\boldsymbol{A}_\perp}{\partial\xi}, \tag{17}$$

$$\boldsymbol{B}_\perp=\nabla_\perp\times(A_z\hat{z})+\nabla_z\times\boldsymbol{A}_\perp. \tag{18}$$

Therefore, the wakefield E_z is completely described in terms of ψ, which can be obtained from a Poisson-like equation whose source term depends only on the profiles of plasma charge density ρ and parallel current J_z, which in turn depend on all the fields through the equation of motion.

III. ON BLOWOUT AND SHEET CROSSING

In this section we will use the simplified sheet (ring) model of Dawson to obtain a condition for trajectory crossing which is valid for weakly driven wakefields. In the next section, we will apply the full set of equations towards describing nonlinear 3D relativistic wakefields. The trajectory crossing condition also defines the transition from the linear regime to the weakly blown-out regime. Imagine electrons that begin at different radial positions. If no trajectory crossing occurs then each electron will always see other electrons at smaller radii and hence there is no region void of electrons. However, if the trajectory of an electron with a sufficiently small initial radius crosses that of another electron, then for radii smaller than this it is possible for an ion column to form. So, trajectory crossing is a necessary but not sufficient condition to reach the blowout regime. As we will show, it provides a very reasonable estimate.

To use the Dawson sheet or ring model we assume a cylindrically symmetric, narrow, bi-flat-top electron driver. We also start by assuming that plasma electron rings do not cross each other. We also assume that the plasma current-induced fields are negligible and that the velocities of the plasma electrons remain nonrelativistic. These assumptions are rigorously valid for low charge drivers and we will quantify what is meant by this later.

The charge density profile for our bi-flat-top model is $n_b(r,\xi)=n_b$ when $r<a$ and $0<\xi<L$, otherwise $n_b(r,\xi)=0$. L is the beam length and a is the beam spot size. In the narrow beam limit we also assume $a\ll 1$ and $L\sim 1$.

The equation of motion for an electron ring can be derived from Eq. (9) by taking the nonrelativistic limit ($v_z \ll v_\perp \ll 1$, $v_\perp\approx dr/d\xi$), and by assuming that the total force on an electron ring is due solely to the electrostatic force from the total charge within the ring, which includes the ion charge, the electron beam charge, and the plasma electron charge,

Downloaded 06 Jun 2006 to 198.11.27.24. Redistribution subject to AIP license or copyright, see http://pop.aip.org/pop/copyright.jsp

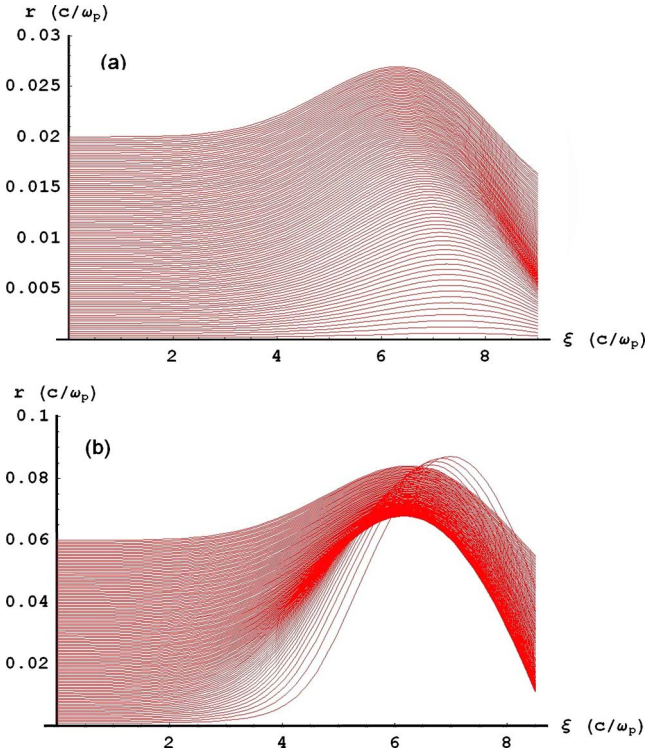

FIG. 2. (Color online) Plots of trajectories for electrons at different initial radial position for an electron beam driver with $k_p\sigma_r=0.01$, $k_p\sigma_z=\sqrt{2}$, the beam center $\xi_0=5$, and with (a) $n_{b0}=1$, (b) $n_{b0}=10$.

$$\frac{d^2r}{d\xi^2}=-\frac{1}{2}r+\frac{c(r_0,r,\xi)}{r}. \tag{19}$$

Here the force term $-r/2$ comes from the uniform ion background. The force term c/r comes from the two-dimensional (2D) cylindrical electrostatic force from the total electron charge inside the ring, where $c(r_0,r,\xi)$ is the total electron charge per unit length within the sheet with a initial position r_0 and a position r at ξ. With the assumption of no crossing, $c(r_0,r,\xi)=\frac{1}{2}r_0^2+\int_0^r r' n_b(r',\xi)dr'$. For the bi-flat-top model and a particle with $r_0>a$, $c(r_0,r,\xi)=\frac{1}{2}(r_0^2+n_b a^2)$.

This equation can be easily integrated numerically. Figure 2 shows two trajectory plots for different n_{b0} for a bi-Gaussian beam driver with $k_p\sigma_r=0.01$ and $k_p\sigma_z=\sqrt{2}$. In Fig. 2(a) $n_{b0}=1.0$ and there is no trajectory crossing, while in Fig. 2(b) $n_{b0}=10$, clear trajectory crossing can be seen.

Clearly there is a transition from no crossing to crossing. We can derive such a condition if we calculate the maximum radius $r_m(r_0)$ for an arbitrary initial radius r_0. This is possible because the particle trajectories all oscillate with frequencies in the variable ξ that are very close to each other, so they will each reach their maxima at nearly the same value of ξ. This effect can also be seen in the above figures. Trajectory crossing occurs when $r_m(r_0)$ changes from a monotonically increasing function to a function with both a local maxima and minima.

First we treat the case $r_0\geqslant a$. The equation of motion can be integrated once leading to the potential energy $\phi(r,r_0)$ for a particle with an initial radius r_0,

$$\phi(r,r_0)=-\frac{1}{4}r^2+\frac{1}{4}\left(\frac{n_b a^2}{r_0^2}+1\right)r_0^2\left(1+2\ln\left(\frac{r}{r_0}\right)\right). \tag{20}$$

A particle's velocity is 0 for both $r=r_0$ and $r=r_m(r_0)$, so the potential for these two radii should be the same,

$$\phi(r_m(r_0),r_0)=\phi(r_0,r_0). \tag{21}$$

This leads to the following relation between $r_m(r_0)$ and r_0:

$$r_m^2-r_0^2=\left(\frac{n_b a^2}{r_0^2}+1\right)r_0^2\ln\frac{r_m^2}{r_0^2}. \tag{22}$$

Rewriting this equation by normalizing the radius to a, $\bar{r}_m=r_m/a$ and $\bar{r}_0=r_0/a$, gives

$$\bar{r}_m^2-\bar{r}_0^2=\left(\frac{n_b}{\bar{r}_0^2}+1\right)\bar{r}_0^2\ln\frac{\bar{r}_m^2}{\bar{r}_0^2}. \tag{23}$$

For the noncrossing assumption to be valid, we need $\bar{r}_m(\bar{r}_0)$ to be a monotonically increasing function of $\bar{r}_0$, this is equivalent to $d\bar{r}_m/d\bar{r}_0>0$. By differentiating the above equation we can get

$$\frac{d\bar{r}_m}{d\bar{r}_0}=\frac{\bar{r}_m}{\bar{r}_0}\left(\ln\frac{\bar{r}_m^2}{\bar{r}_0^2}-\frac{n_b}{\bar{r}_0^2}\right)\left(\ln\frac{\bar{r}_m^2}{\bar{r}_0^2}-\frac{n_b}{\bar{r}_0^2}+\frac{n_b}{\bar{r}_0^2}\ln\frac{\bar{r}_m^2}{\bar{r}_0^2}\right)^{-1}. \tag{24}$$

There is no particle crossing for sufficiently large $\bar{r}_0$ since $d\bar{r}_m/d\bar{r}_0\to 1$ as $\bar{r}_0\to\infty$. We see that for $\ln\bar{r}_m^2/\bar{r}_0^2=n_b/\bar{r}_0^2$ we have $d\bar{r}_m/d\bar{r}_0=0$, which defines the onset of particle crossing. We denote this critical $\bar{r}_0$ as $\bar{r}_{0m}$. Combined with the above equation, this gives $\bar{r}_{0m}$ and $\bar{r}_m(\bar{r}_{0m})$ for a given n_b. We find that $u\equiv n_b/\bar{r}_{0m}^2$ satisfies the following equation:

$$\exp(u)-1=u(u+1). \tag{25}$$

This equation has a nonzero solution $u_0=1.7933$. Correspondingly, $\bar{r}_{0m}=0.747\sqrt{n_b}$ and $\bar{r}_m(\bar{r}_{0m})=1.831\sqrt{n_b}$. In our analysis $\bar{r}_0\geqslant 1$, therefore only when $n_b\geqslant 1.792$ can particle crossing be possible. We can verify that at this $\bar{r}_{0m}$, $\bar{r}_m$ is a minimum by checking if $d^2\bar{r}_m/d\bar{r}_0^2>0$. Differentiating Eq. (24) we get

$$\frac{d^2\bar{r}_m}{d\bar{r}_0^2}=\frac{2\bar{r}_m\bar{r}_0^2}{n_b^2}\left(\frac{n_b}{\bar{r}_0^2}-1\right), \tag{26}$$

which is obviously greater than 0, since we have $n_b/\bar{r}_{0m}^2=1.7933$.

For $r_0<a$, a similar calculation can be carried out by taking into account the kinetic energy of the particle when it reaches $r=a$. Some particles very close to the axis will not reach $r=a$; for example, the particle with $r_0=0$ will just go through the beam without any deflection. This is very similar to an unstable equilibrium, where every trajectory with an initial r_0 slightly different than 0 will leave the equilibrium very quickly.

It turns out that for a beam density smaller than a critical density (surprisingly the same value $n_b=1.792$), $r_m(r_0)$ is a monotonically increasing function. Assuming $r_0<a$, then for $n_b>1.792$, $r_m(r_0)$ $(r_0<a)$ will have a local maximum at

Downloaded 06 Jun 2006 to 198.11.27.24. Redistribution subject to AIP license or copyright, see http://pop.aip.org/pop/copyright.jsp

some radius $r_0=r^*<a$. If we keep increasing n_b, this r^* will move toward 0, which means more electrons inside the beam will be blown out.

Combining the results for $r_0<a$ and $r_0>a$, we can make the following conclusions:

(1) When the beam density satisfies the condition, $n_b<1.792$, then $r_m(r_0)$ is a monotonically increasing function. In this case, no particle crossing happens.
(2) If $n_b>1.792$, then $r_m(r_0)$ will have a negative slope between $r^*<r_0<r_{0m}$, where $r^*<a$ is a local maximum of $r_m(r_0)$, and $r_{0m}>a$ is a local minimum of $r_m(r_0)$. In addition, $r_m(r_{0m})$ is the blowout radius. Electrons with initial positions in this range will cross an electron that starts at position at r_{0m}. If n_b is large enough (e.g., $n_b=10$), r^* will also be very close to 0, which means almost all electrons of $r_0<r_{0m}$ will cross electrons with $r_0=r_{0m}$, so a nearly pure ion channel will be formed.

We can rewrite the blowout radius $r_{\max}$ in normalized units as

$$r_{\max}=1.831(n_b a^2)^{1/2}. \tag{27}$$

We define Λ as normalized charge per unit length,

$$\Lambda \equiv \int_0^\infty r n_b dr. \tag{28}$$

For a bi-flat-top beam, $\Lambda=n_{b0}a^2/2$, and for a bi-Gaussian beam, $\Lambda=n_{b0}\sigma_r^2$. The blowout radius then can be written as $r_{\max}=2.58\Lambda^{1/2}$. This basically shows that in the blowout regime the blowout radius depends primarily on the total charge per unit length and not just the peak density. It is worth noting that for a bi-Gaussian beam ($\sigma_z\sim 1$ and $\sigma_r\ll 1$), simulations and trajectory calculations show that $r_{\max}\approx 2(n_{b0}\sigma_r^2)^{1/2}$, which is about 20% smaller than the above theoretical value. The reason is that the bi-Gaussian beam has a longitudinally varying density profile, but the formula uses the maximum density leading to a larger result.

For a very short driver, e.g., $L\ll 1$, it is the initial kick from the beam that determines if blowout will happen or not. A similar calculation to that given above can be carried out. The main difference is that for this case it is the total charge of the beam that determines the condition for blowout and the blowout radius. The relation between the blowout radius and the total charge Q also has similar form, e.g., $r_{\max}\propto Q^{1/2}$.

A direct consequence of complete blowout is the formation of a narrow electron sheath around the blowout boundary. The above method for calculating the blowout radius can also give an estimate for the width of this narrow region. We can get such an estimate by calculating the maximum radius for an electron initially located at the blowout radius, $r_0=r_{\max}$. The result is $1.287r_{\max}$. Therefore, 0.287 can be a rough estimate of the ratio between the width of narrow sheath and the blowout radius. Real density profiles from PIC simulations show that width is actually less, so generally we can treat the width of the narrow sheath as a small fraction of the blowout radius. This will be a key approximation in the theoretical model for blowout regime given in the next section.

IV. WAKE EXCITATION IN THE BLOWOUT REGIME

In the previous sections, we have presented the basic theoretical framework for wake excitation and some physical insight for the blowout regime. In this section we use this framework and insight to develop a general model for wakefields in the blowout regime. The key approximation is based on the observation that the plasma density and current profile can be roughly divided into three distinct regions: an ion channel, a narrow plasma electron sheath, and a linear-response region where the perturbation of the plasma is very weak. The ion channel has a sharp boundary; that is, at the blowout radius the electron density rises from 0 to a large value in an essentially infinitesimal distance. For much of the ion channel, the channel boundary, $r_b(\xi)$, is also the trajectory of the most inner electron. The plasma electron density and axial current density profiles in the narrow electron sheath are rather narrow at $r_b(\xi)$ and the width $\Delta_s(\xi)$ is small compared with $r_b(\xi)$ for most part of the ion channel except where r_b is very close to zero. Indeed the profiles are more like exponential decay than constant. Beyond the narrow sheath, the perturbation of plasma density and current becomes very weak, so this region can be described by a linear fluid model. From linear theory, we know this region has a typical width around one plasma skin depth c/ω_p. The contribution to the wakefield from the linear-response region must be taken into account due to its rather large width. For small blowout radius the contribution from this outer linear-response region is dominant.

At this point, we will assume the wake is excited by a bi-Gaussian electron driver with a density profile

$$n_b(r,\xi)=\frac{N}{(2\pi)^{3/2}\sigma_r^2\sigma_z}e^{-r^2/2\sigma_r^2}e^{-\xi^2/2\sigma_z^2}. \tag{29}$$

How the formalism is modified for a laser driver will be addressed later. In addition, for laser drivers the assumption that the sheath is narrow is not necessarily valid. By assuming azimuthal symmetry, we can rapidly obtain solutions for Eqs. (7) and (13) because of their Poisson-like form. Inside the ion channel, i.e., for $r\leqslant r_b$ and for $r\gg\sigma_r$,

$$\phi=\phi_0(\xi)-\frac{r^2}{4}+\lambda(\xi)\ln r, \tag{30}$$

$$A_z=A_{z0}(\xi)+\lambda(\xi)\ln r, \tag{31}$$

where $\lambda(\xi)=\int_0^{r\gg\sigma_r} r n_b dr$ and $\phi_0(\xi)\equiv\phi(r=0,\xi)$, and $A_{z0}(\xi)\equiv A_z(r=0,\xi)$. In addition,

$$A_r=\sigma(\xi)r, \tag{32}$$

where from the gauge condition,

$$\sigma(\xi)=-\frac{1}{2}\frac{d}{d\xi}\psi_0(\xi)=-\frac{1}{2}E_{z0}, \tag{33}$$

$$\psi=\psi_0-\frac{r^2}{4}. \tag{34}$$

Downloaded 06 Jun 2006 to 198.11.27.24. Redistribution subject to AIP license or copyright, see http://pop.aip.org/pop/copyright.jsp

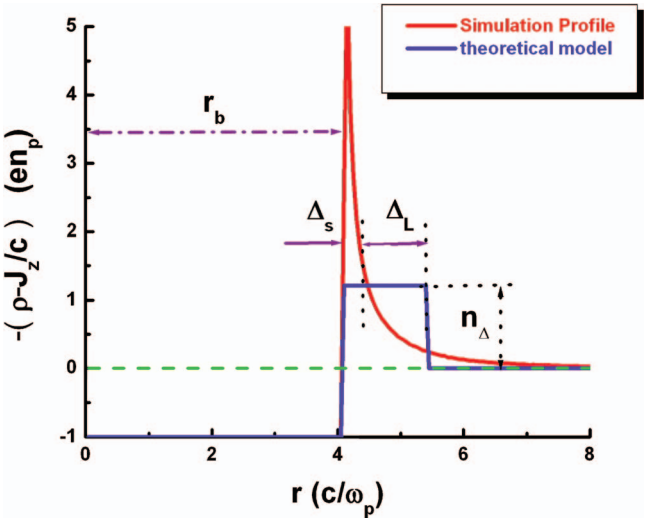

FIG. 3. (Color) $J_z/c-\rho$ profile from a PIC simulation.

We have also assumed that the beam is highly relativistic, i.e., $\rho_b - J_b = \rho_b(1-v_{zb}) \to 0$. The force on a plasma electron at $r=r_b(\xi)$, or for a beam electron, can therefore be written as

$$F_\perp = -(E_r - V_z B_\theta) = \frac{\partial \phi}{\partial r} - V_z \frac{\partial A_z}{\partial r} + (1-V_z)\frac{\partial A_r}{\partial \xi}$$

$$= -\frac{1}{2}r + (1-V_z)\frac{\lambda(\xi)}{r} + (1-V_z)\frac{d\sigma}{d\xi}r, \tag{35}$$

where the first term is due to the space charge of the unshielded ion channel, and the second and the third terms are due to the electric and magnetic fields from the electron beam and to plasma radial currents, respectively. Note that the focusing force on a beam electron with $V_z \sim 1$ is due solely to the space charge of the ion channel because the electric and magnetic forces from the plasma currents and the beam's self-forces each cancel. On the other hand, for plasma electrons for which $-1 < V_z \ll 1$ the force is due to the full electromagnetic character of the wake. In order to uniquely calculate the force on a plasma electron at $r=r_b(\xi)$, we next need to calculate $\sigma(\xi)$ or, equivalently, $\psi_0(\xi)$.

The source term for $\psi(r,\xi)$ is $\rho - J_z$. From the continuity equation it follows that

$$\frac{d}{d\xi}\int r(\rho - J_z)dr = 0. \tag{36}$$

Far in front of the electron beam where the plasma is unperturbed $\rho - J_z = 0$ so $\int r(\rho - J_z)dr = 0$ for all ξ. This is a critical condition because it grants ψ a global definition. At each ξ we assume

$$\rho - J_z = \rho_{\text{ion}} + \rho_e - J_{ze}, \tag{37}$$

where $\rho_{\text{ion}}=1$ for all r and $\rho_e - J_{ze}$ is zero for $r<r_b$, rises sharply within a sheath of thickness of Δ_s and gradually falls to unity in a width Δ_L. The region defined by Δ_L is where the plasma electrons respond nearly as they would have in a linear wake. This is illustrated in Fig. 3, where the profile $J_z/c-\rho$ versus. r is plotted for an arbitrary value of ξ from Fig. 1. It does not appear possible to analytically determine the exact profiles of $\rho - J_z$ within the sheath and linear regions. However, the results are very insensitive to the forms of the profiles and we find that very accurate results can be obtained by assuming $J_z - \rho = -1$ for $r < r_b$ and is a constant

$$n_\Delta = \frac{r_b^2}{(r_b+\Delta)^2 - r_b^2} \tag{38}$$

for $r_b < r < r_b + \Delta$, where $\Delta \equiv \Delta_s + \Delta_L$. This is illustrated in Fig. 3. Obviously, more refined profiles can be used. Under these assumptions

$$\psi = \frac{r_b^2(\xi)}{4}(1+\beta(\xi)) - \frac{r^2}{4} \tag{39}$$

for $r \leqslant r_b$, where

$$\beta(\xi) = \frac{(1+\alpha)^2 \ln(1+\alpha)^2}{(1+\alpha)^2 - 1} - 1, \tag{40}$$

$$\alpha \equiv \frac{\Delta}{r_b} = \frac{\Delta_L}{r_b} + \frac{\Delta_s}{r_b}. \tag{41}$$

We assume $\Delta_s / r_b \equiv \epsilon \ll 1$ except at the back of the blowout region where $r_b \ll 1$. To complete the analysis, we use these results to derive a single equation for $r_b(\xi)$ by using the relativistic equation of motion for a plasma electron,

$$\frac{dP_\perp}{d\xi} = \frac{1}{1-V_z}F_\perp. \tag{42}$$

We can rewrite the left-hand side as

$$\frac{dP_\perp}{d\xi} = \frac{d\gamma V_\perp}{d\xi} = \frac{d}{d\xi}\gamma(1-V_z)\frac{d}{d\xi}r_\perp = \frac{d}{d\xi}(1+\psi)\frac{d}{d\xi}r_\perp, \tag{43}$$

and use the expression for $1-V_z$ from Eq. (12). The equation of motion for a plasma particle at r_b can now be written as

$$\frac{d}{d\xi}\left[(1+\psi)\frac{d}{d\xi}r_b\right] = r_b\left\{-\frac{1}{4}\left[1 + \frac{1}{(1+\psi)^2} + \left(\frac{dr_b}{d\xi}\right)^2\right] + \left(\frac{d\sigma}{d\xi}\right) + \frac{\lambda(\xi)}{r_b^2}\right\}, \tag{44}$$

where $\psi(r_b(\xi))$ is given by Eq. (39). This can be simplified further if we assume that ϵ and Δ_L depend weakly on ξ, e.g.,

$$\frac{\partial \epsilon}{\partial \xi} \approx 0, \quad \frac{\partial \Delta_L}{\partial \xi} \approx 0 \tag{45}$$

so that $d\beta/d\xi = dr_b/d\xi \partial\beta/\partial r_b$. Under this assumption Eq. (44) reduces to

$$A(r_b)\frac{d^2 r_b}{d\xi^2} + B(r_b) r_b \left(\frac{dr_b}{d\xi}\right)^2 + C(r_b) r_b = \frac{\lambda(\xi)}{r_b}, \tag{46}$$

where

Downloaded 06 Jun 2006 to 198.11.27.24. Redistribution subject to AIP license or copyright, see http://pop.aip.org/pop/copyright.jsp

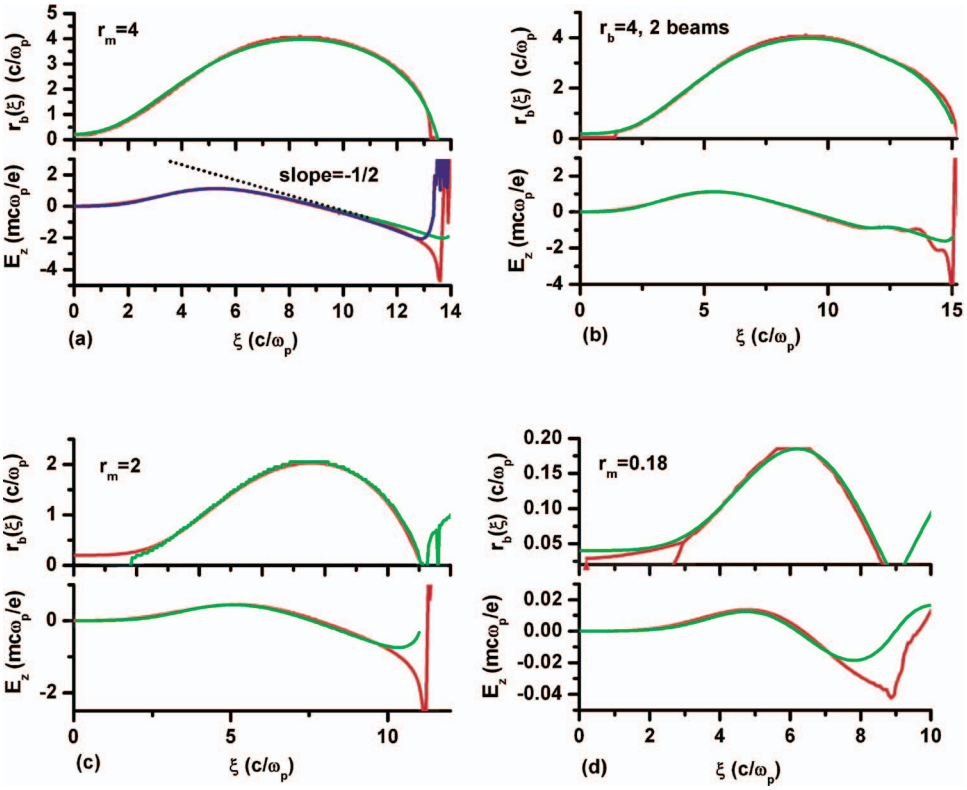

FIG. 4. (Color) Comparison of the trajectories of $r_b(\xi)$ and the accelerating field $E_z(\xi)$ between theoretical calculations and PIC simulations: PIC simulation (red), calculation using a constant profile (green), and calculation using a varying profile (blue). The maximum blowout radius is (a) $r_m=4$; (b) $r_m=4$ with two beams; (c) $r_m=2$; and (d) $r_m=0.18$.

$$A(r_b) = 1 + \left[\frac{1}{4} + \frac{\beta}{2} + \frac{1}{8} r_b \frac{d\beta}{dr_b}\right] r_b^2,$$

$$B(r_b) = \frac{1}{2} + \frac{3}{4}\beta + \frac{3}{4} r_b \frac{d\beta}{dr_b} + \frac{1}{8} r_b^2 \frac{d^2\beta}{dr_b^2},$$

$$C(r_b) = \frac{1}{4}\left[1 + \frac{1}{\left(1 + \frac{\beta}{4} r_b^2\right)^2}\right].$$

Recall that once $r_b(\xi)$ is solved for, then $\psi(r,\xi)$ is known [Eq. (39)] and

$$E_z(r,\xi) = \frac{d}{d\xi}\psi(r=0,\xi) = \frac{d}{d\xi}\left[\frac{1}{4} r_b^2 (1+\beta(\xi))\right] \tag{47}$$

is known. We note here that for a laser driver $C(r_b)=[1+(1+a^2/2)/(1+\beta r_b^2/4)^2]/4$ and the right-hand side of Eq. (46) becomes $-d[|a|^2/4]/dr/[1+\beta r_b^2/4]$, which comes from the laser's ponderomotive force.

We show the accuracy of our model by directly integrating Eq. (46) for a bi-Gaussian electron beam driver. We choose $k_p\sigma_r=0.1$ and $k_p\sigma_z=\sqrt{2}$. In Fig. 4, we plot the trajectories of $r_b(\xi)$ for different values of beam charge, i.e., eN, and hence different maximum blowout radius (r_m varies from 0.18 to 4) and compare these trajectories with the ion channel boundaries extracted from fully nonlinear PIC simulations. The theory and PIC simulation results for r_b are essentially identical for each case. We used $\Delta_s=0.1r_b$ and $\Delta_L=1$ for each case. Varying Δ_L from 0 to 3 leads to only a 20% deviation in both the blowout radius and the ion channel length. Figure 4 also compares the wakefields, E_z, calculated from the model with those from PIC simulations. The agreement is excellent until near the rear of the blowout region (large values of ξ). We have determined that much of the disagreement comes from assuming constant Δ_s/r_b and Δ_L, which is not exactly true near the rear of the first bucket where r_b becomes small. In Fig. 4(a), we also plot the wakefield, E_z, which is calculated using a Δ_L which depends on ξ. This gives better agreement near the rear of the ion column. Although this simple model cannot give exact predictions for E_z near the very rear of the ion channel, it provides the correct trajectory for r_b and hence the correct structure of the wakefield, e.g., the peak decelerating field, the useful accelerating field, the useful transformer ratio, and the wake's wavelength for arbitrary shaped bunches. It also describes quantitatively how the wakefield's structure changes as r_m increases. We also note that it is accurate enough to treat the beam-loading problem. Figure 4(b) shows the agreement between the theory and simulation where a drive beam and a trailing beam are used. The agreement is exact within the trailing beam. More details on beam loading will be given in a separate publication.

Much can be learned by examining Eq. (46) in two distinct limits: namely the nonrelativistic blowout regime where $r_m \ll 1$, and the ultrarelativistic blowout regime where $r_m \gg 1$. Before providing details on these two distinct regimes in the following two sections, we summarize some key features.

In the ion channel, $r < r_b$, the wakefield $E_z(r,\xi)$ can be expressed as

$$E_z(r,\xi) = \frac{\partial}{\partial\xi}\psi(0,\xi). \tag{48}$$

Downloaded 06 Jun 2006 to 198.11.27.24. Redistribution subject to AIP license or copyright, see http://pop.aip.org/pop/copyright.jsp

All three plasma regions (ion channel, narrow electron sheath, and the linear-response region) contribute to $\psi(0,\xi)$,

$$\psi(0,\xi) = \int_0^\infty \frac{dr}{r}\int_0^r (\rho - J_z/c)r'dr' = \left\{\int_0^{r_b} + \int_{r_b}^{r_b+\Delta_s} + \int_{r_b+\Delta_s}^{\infty}\right\}\left[\frac{dr}{r}\int_0^r (\rho - J_z/c)r'dr'\right] = \psi_{\rm ion} + \psi_s + \psi_{\rm linear}, \quad (49)$$

where $\psi_{\rm ion}=r_b^2/4$ is the part contributed by ion channel and ψ_s is the part contributed by the narrow electron sheath. Because the width of the sheath is small compared with r_b for almost all values of ξ, ψ_s is a small fraction of $\psi_{\rm ion}$. The third term, $\psi_{\rm linear}$, is the part contributed by the linear-response region. This is a region of width around 1 (c/ω_p in unnormalized units), so its relevant importance depends on the blowout radius r_m. If $r_m \gg 1$ (the ultrarelativistic blowout), it will be much smaller than $\psi_{\rm ion}$. If $r_m \ll 1$ (the nonrelativistic blowout), it will be the dominating part.

We can estimate the form of $\beta(\xi)$ in the following two limits:

When $r_m \gg 1$ the ratio $\alpha \ll 1$, providing

$$\beta(\xi) \approx \alpha. \quad (50)$$

We can see that in this limit the ion channel is the dominant contribution to $\psi(0,\xi)$ because $\beta(\xi)\approx\alpha\ll 1$.

On the other hand, when $r_m \ll 1$ the ratio $\alpha \gg 1$, leading to

$$\beta(\xi) \approx 2\ln\alpha. \quad (51)$$

This logarithmic term provides a direct connection between linear fluid theory and the linear-response region. In this limit, the contribution from the linear region is now much larger than that from the ion channel.

V. ON THE TRANSITION BETWEEN LINEAR THEORY AND THE BREAKDOWN OF FLUID THEORY

In this section we use the results in the previous section for $r_m \ll 1$ to make a connection between blowout theory and the results of linear fluid theory.

In the linear fluid theory[5] for a narrow short electron driver (e.g., $k_p\sigma_z=\sqrt{2}$ and $k_p\sigma_r \ll 1$), the maximum wakefield $E_{z\,\max}$ can be written as

$$\frac{eE_{z\,\max}}{mc\omega_p} \approx 1.3\frac{n_{b0}}{n_p}k_p^2\sigma_r^2\ln\frac{1}{k_p\sigma_r}. \quad (52)$$

This formula has a logarithmically divergent term, $\ln 1/k_p\sigma_r$. If we fix the charge per unit length $\Lambda \equiv n_{b0}/n_p k_p^2\sigma_r^2$ and keep decreasing the beam spot size $k_p\sigma_r$, Eq. (52) predicts the wakefield will blow up. Indeed this divergence inherently exists in the Green's function of the wakefield for a point charge.

This nonphysical infinity arises from the breakdown of linear fluid theory. When the spot size decreases, the beam density also increases, and eventually will become larger than the background plasma density. When the beam density is much larger than the plasma density, clear blowout will happen and the wakefield will saturate. Recently,[5] we showed through PIC simulations that such a saturation happens at $n_{b0}/n_p \sim 10$, where a clear blowout occurs at the front of the beam. We found[5] that an approximate formula for the wakefield after clear blowout has the following form:

$$\frac{eE_{z\,\max}}{mc\omega_p} \approx 1.3\Lambda\ln\frac{1}{\sqrt{\Lambda/10}}. \quad (53)$$

Based on the present theory, it is easy to understand such a logarithmic dependence on Λ. Once the beam spot size has decreased to a value such that clear blowout occurs, decreasing the beam spot size further will not change the plasma response to the beam. The linear-response region beyond the maximum blowout radius r_m ($k_p r_m \approx 2\sqrt{\Lambda}$, as shown in Sec. III) will give such a logarithmic dependence.

In the nonrelativistic blowout regime ($r_m \ll 1$), the plasma current-induced fields (e.g., $\partial A_r/\partial\xi$) are of second order as compared with space-charge fields (e.g., $\partial\phi/\partial r$). In the linear-response region no trajectory crossing occurs so plasma electrons only feel the electric forces from the beam and the ions that they cross. Therefore, the plasma response in the region $r > r_m+\Delta_s$ is the same as it would be from a wider low density beam with the same Λ but with a width $r_m+\Delta_s$. Therefore, we can calculate an expression for $\psi_{\rm linear}$ from linear theory.

For simplicity, we calculate this $\psi_{\rm linear}$ for a bi-flat-top beam with spot size a, length L, and density n_{b0} ($a\ll 1$, $L\approx 2\pi$).

From the linear theory,[5] $E_z(r,\xi)$ for this beam profile is

$$E_z(r,\xi) = n_{b0}R(r)\sin\xi, \quad (54)$$

where $R(r)=\int_0^\infty n_b(r')I_0(r_<)K_0(r_>)r'dr'$ is the radial function of the linear wakefield. Integrating this along ξ we get

$$\psi(r,\xi) = n_{b0}R(r)(1-\cos\xi). \quad (55)$$

$R(r)$ can be expanded for $a\ll 1$ and $r\ll 1$,

$$R(r) \approx R(0) - \frac{1}{4}(1-R(0))r^2, \quad (56)$$

where

$$R(0) \approx \frac{a^2}{2}\ln\left(\frac{1.85}{a}\right). \quad (57)$$

For $a=r_m+\Delta_s\approx r_m$ and $n_{b0}=2\Lambda/r_m^2$, we get

$$\psi_{\rm linear}(\xi) \approx 2\Lambda\ln\left(\frac{1.12}{r_m}\right)\left(\frac{1-\cos\xi}{2}\right). \quad (58)$$

This expression reaches its maximum of $2\Lambda\ln(1.12/r_m)$ at $\xi=\pi$, which is also where $r_b(\xi)$ reaches its maximum r_m. We can combine the three contributions to $\psi(0,\xi)$ and get $\psi(0,\xi)$ near the maximum blowout radius r_m ($\xi\approx\pi$),

$$\psi(0,\xi) \approx 2\Lambda\ln\left(\frac{1.12}{r_m}\right)\left(\frac{1-\cos\xi}{2}\right) + (1+\epsilon(\xi))\frac{r_b^2}{4}, \quad (59)$$

where $\epsilon\equiv\Delta_s/r_b$. The wakefield E_z in the ion channel is therefore

Downloaded 06 Jun 2006 to 198.11.27.24. Redistribution subject to AIP license or copyright, see http://pop.aip.org/pop/copyright.jsp

$$E_z(r,\xi) \approx \frac{1+\epsilon(\xi)}{2} r_b(\xi)\frac{d}{d\xi}r_b(\xi) + 2\Lambda \ln\left(\frac{1.12}{r_m}\right)\frac{\sin\xi}{2}. \tag{60}$$

For small r_b, the equation of motion for $r_b(\xi)$, Eq. (46), can be reduced to

$$\frac{d^2 r_b}{d\xi^2} = -\frac{1}{2}r_b + \frac{\lambda(\xi)}{r_b}, \tag{61}$$

which is identical to Eq. (19). At the maximum blowout where $\xi=\xi_0\approx\pi$, $dr_b/d\xi=0$. Therefore, to first order in $(\xi-\xi_0)$,

$$r_b(\xi)\frac{d}{d\xi}r_b(\xi) \approx r_m \frac{d^2 r_b}{d^2\xi}(\xi_0)(\xi-\xi_0). \tag{62}$$

It thus follows that to lowest order, $E_z(r,\xi)$ is

$$E_z(r,\xi) \approx -\left(\frac{1}{4}r_m^2(1+\epsilon)\left(1-\frac{2c(\xi_0)}{r_m^2}\right)+\Lambda\ln\left(\frac{1.12}{r_m}\right)\right) \times(\xi-\xi_0). \tag{63}$$

Substituting $r_m\approx 2.58\Lambda^{1/2}$ into the above expression for E_z, and also noting that ϵ and $2c(\xi_0)/r_m^2$ are both small, we obtain

$$E_z(r,\xi) \approx -\left(\Lambda\ln\left(\frac{1}{\sqrt{\Lambda/5.3}}\right)\right)(\xi-\xi_0). \tag{64}$$

For very small blowout radius, the wakefield structure is close to a sinusoidal form, so the slope at the point where $E_z=0$ can be used to roughly determine the maximum wake amplitude. This gives

$$E_{z\,\max} \approx \Lambda\ln\left(\frac{1}{\sqrt{\Lambda/5.3}}\right). \tag{65}$$

Although this is calculated for a bi-flat-top beam, we can see it is very close to the formula given in Eq. (53), which was deduced from simulations.[5]

VI. ULTRARELATIVISTIC BLOWOUT REGIME

In the ultrarelativistic limit where $r_m\gg 1$, $\beta\ll 1$ and $\beta r_m^2\gtrsim 4$, Eq. (46) reduces to

$$r_b\frac{d^2 r_b}{d\xi^2} + 2\left[\frac{dr_b}{d\xi}\right]^2 + 1 = \frac{4\lambda(\xi)}{r_b^2}. \tag{66}$$

The bunch length is typically much shorter than the nonlinear ion channel length, so we can ignore the driving term on the right-hand side for much of the trajectory. The equation for a circle is

$$r_b\frac{d^2 r_b}{d\xi^2} + \left[\frac{dr_b}{d\xi}\right]^2 + 1 = 0, \tag{67}$$

while Eq. (66) gives

$$r_b\frac{d^2 r_b}{d\xi^2} + 2\left[\frac{dr_b}{d\xi}\right]^2 + 1 = 0, \tag{68}$$

with the right-hand side set to zero. Near the top of a circle $dr_b/d\xi\to 0$, so the trajectory $r_b(\xi)$ maps out a circle until the rear of the blowout region. The effect of the "extra" $[dr_b/d\xi]^2$ term is to bend the trajectory downward more quickly as $dr_b/d\xi$ becomes large. This is indeed what is observed in Fig. 4(a). We can rewrite the left-hand side of Eq. (66) as

$$\frac{d}{d\xi}\left[\frac{1}{2}r_b\frac{dr_b}{d\xi}\right] = -\frac{1}{2} - \frac{1}{2}\left[\frac{dr_b}{d\xi}\right]^2, \tag{69}$$

and since it follows from Eq. (47) that $E_z(\xi)\approx 1/2 r_b dr_b/d\xi$ when $\beta(\xi)$ can be neglected for $r_b\gg 1$, we see that E_z has a slope $\partial E/\partial\xi=-1/2$ at the top of the channel and the slope increases as $dr_b/d\xi$ increases, leading to the characteristic spike. This is seen in Fig. 4(a) where a line with a slope of $-1/2$ is shown for convenience.

For most situations of interest, the driver is sufficiently short that the right-hand side of Eqs. (46) and (66) can be neglected at the point where $r_b(\xi_0)=r_m$. For $\xi>\xi_0$ and for $r_m\gtrsim 4$ the trajectory for r_b maps out a circle and the ion column is a sphere, i.e., a bubble. The value of $E_z=0$ at $\xi=\xi_0$, and E_z decreases linearly from 0 to $-r_m/2$ in a distance $L_c=r_m$. Therefore the nonlinear frequency (or wave number) is $\omega_{NL}=\pi/r_m\omega_p$ and in terms of the amplitude $E_{z\max}=r_m/2$, $\omega_{NL}=\pi/2E_{z\max}\omega_p$. Interestingly the same relationship holds for nonlinear one-dimensional plasma oscillations[1] although the physics is completely different. In these 3D wakes the wakefields are electromagnetic in character. Besides the accelerating axial electric field, E_z, there are transverse electric fields, E_r, and magnetic fields, B_θ. The E_r fields come from the ion column, $E_{r\text{ion}}=1/2r$, and the radial plasma current, $E_{rEM}=-1/4r$, while B_θ comes from the radial plasma current, $B_{\theta EM}=-1/4r$. The total focusing field on a beam electron is $E_r-B_\theta=1/2r=E_{r\text{ion}}$.

VII. FORMULAS FOR ARBITRARY BLOWOUT RADIUS

We can also get expressions for arbitrary blowout radius by taking into account all the terms in the equation of motion. First we can get the slope of the wakefield near the top of the ion channel by expanding the equation of motion near the maximum blowout radius. From Eq. (45) the wakefield inside the ion channel is

$$E_z(\xi) = \frac{d}{d\xi}\psi(0,\xi) = \left(\frac{1}{2}+\frac{1}{2}\beta+\frac{1}{4}r_b\frac{d\beta}{dr_b}\right)r_b\frac{dr_b}{d\xi}. \tag{70}$$

At the maximum blowout radius $\xi=\xi_m$, $r_b=r_m$ and $dr_b/d\xi=0$. The blowout radius $r_b(\xi)$ can then be expanded about $\xi=\xi_m$,

$$r_b(\xi) \approx r_m + \frac{1}{2}\frac{d^2 r_b}{d\xi^2}(\xi_m)(\xi-\xi_m)^2. \tag{71}$$

This leads to

$$\frac{dr_b}{d\xi} \approx \frac{d^2 r_b}{d\xi^2}(\xi_m)(\xi-\xi_m) \tag{72}$$

and

Downloaded 06 Jun 2006 to 198.11.27.24. Redistribution subject to AIP license or copyright, see http://pop.aip.org/pop/copyright.jsp

$$E_z(\xi) \approx \left[\frac{1}{2} + \frac{1}{2}\beta(r_m) + \frac{1}{4} r_m \frac{d\beta}{dr_b}(r_m)\right] r_m \frac{d^2 r_b}{d\xi^2}(\xi_m)(\xi - \xi_m). \tag{73}$$

From the equation of motion for r_b,

$$\frac{d^2 r_b}{d\xi^2}(r_m) = -\frac{\left[C(r_m) - \frac{\lambda(\xi_m)}{r_m^2}\right]}{A(r_m)} r_m. \tag{74}$$

So the slope of E_z at $\xi = \xi_m$ can be written as

$$\frac{dE_z}{d\xi}(\xi_m) = -\left[\frac{1}{2} + \frac{1}{2}\beta(r_m) + \frac{1}{4} r_m \frac{d\beta}{dr_b}(r_m)\right] \times r_m^2 \frac{\left[\frac{1}{4}\left[1 + \frac{1}{(1+\beta r_m^2)^2}\right] - \frac{\lambda(\xi_m)}{r_m^2}\right]}{1 + \left[\frac{1}{4} + \frac{1}{2}\beta + \frac{1}{8} r_m \frac{d\beta}{dr_b}\right] r_m^2}. \tag{75}$$

We can easily check this formula for the two limits. For nonrelativistic blowout where $r_m \ll 1$, $\beta(r_m) \gg 1$, $\beta(r_m) r_m^2 \ll 1$, and $\frac{1}{4} r_m d\beta / dr_b(r_m) \sim -\frac{1}{2}$, resulting in

$$\frac{dE_z}{d\xi}(\xi_m) \approx -\frac{1}{4}\beta(r_m) r_m^2. \tag{76}$$

By substituting $r_m \sim 2\sqrt{\Lambda}$ and $\beta(r_m) \sim \ln 1/r_m^2$, we can roughly recover the scaling $\Lambda \ln 1/\Lambda$. The wakefield also scales the same way because the wavelength in this limit is a constant. So we can roughly say that in the nonrelativistic blowout regime the accelerating field scales as r_m^2.

On the other hand, for ultrarelativistic blowout where $r_m \gg 1$, $\beta(r_m) \ll 1$, $\beta(r_m) r_m^2 \gg 1$, and $\frac{1}{4} r_m d\beta / dr_b(r_m) \sim \beta(r_m)$, leading to

$$\frac{dE_z}{d\xi}(\xi_m) \approx -\frac{1}{2}. \tag{77}$$

In this limit, the slope is a constant, and the ion channel has a spherical shape, so the accelerating field scales as r_m.

We can also get estimates for the ion channel length for arbitrary blowout radius. For small blowout radius, the half length of the ion channel is fixed at $\pi/\sqrt{2}$. For large blowout radius ($r_m \gtrsim 4$), half of the ion channel length is almost the same as the blowout radius. For a blowout radius between ($1 < r_m < 4$), the ion channel is close to an ellipse, and the half length of this channel can be calculated by assuming a constant wakefield slope.

$$E_z \approx \frac{1}{2}(1 + \beta(r_m)) r_b \frac{dr_b}{d\xi} \approx -k_s \xi. \tag{78}$$

Integrating once gives an equation for an ellipse,

$$r_b^2 + \frac{2k_s}{1+\beta}\xi^2 \approx r_m^2. \tag{79}$$

Evaluating ξ for $r_b = 0$ provides the half length of the ion channel, $L_h \approx \sqrt{1 + \beta/2k_s}\, r_m$.

VIII. DIFFERENCES BETWEEN LASER DRIVER AND BEAM DRIVER

In previous sections, we treated both the laser drivers and the beam drivers on the same footing. We used the same sheath model for each and the analysis indicated that the wake structure is basically dictated by the maximum blowout radius, r_m, so long as the laser or particle beam driver is sufficiently short.

In this section we will discuss the differences between the laser and the beam drivers in several important aspects: driver spot size, blowout radius, and the matching condition.

For the electron driver case, the bunch is typically narrow, $\sigma_r \ll r_m$, and the ultrarelativistic limit is generally not reached, $r_m \sim 2$. For example, in the E164X experiments,[7] $N = 1.8 \times 10^{10}$, $\sigma_z = 30$ μm, $\sigma_r = 10$ μm, and the plasma density was 5×10^{16} cm^{-3}. Therefore $n_b/n_p \approx 7$ and $\Lambda \approx 1$. For these parameters, $k_p r_m \approx 2$. For such an r_m, both the ion channel and linear-response regions contribute significantly to the wake excitation.

For the laser driver case, narrow lasers ($W_0 \omega_p / c \ll 1$) cannot be guided because even a fully evacuated channel cannot provide an index of refraction with enough depth to compensate the laser diffraction. This can be seen from the linear guiding condition. For a transverse Gaussian laser profile with spot size W_0, the normalized channel depth $\Delta n_c / n_p$ needed to guide the laser is[21]

$$\frac{\Delta n_c}{n_p} = \frac{4}{(k_p W_0)^2}. \tag{80}$$

Complete blowout occurs when $\Delta n_c / n_p \sim 1$ and $k_p W_0 > 2$ is the requirement for optical guiding. In order for a laser with such a spot size to cause blowout, the normalized vector potential a_0 also needs to be larger than 1. Therefore, laser powers larger than P_c (the critical power for relativistic self-focusing[22]) are needed to generate blowout. Since the blowout radius will exceed the laser spot size, when using laser drivers, one is often in the ultrarelativistic blowout regime or bubble regime.

Unlike the space-charge force of an electron beam, the ponderomotive force of the laser only extends out to the edge of the laser. For a given laser power P and plasma density n_p, there is a matched spot size which produces well-defined sheaths and good guiding properties for the laser. If the spot size is much larger than this matched size, the normalized vector potential a_0 will be too small to cause blowout initially. However, relativistic self-focusing will also result in the back of the pulse focusing down to a spot size $\sim c/\omega_p$, which will then lead to blowout.[22] Conversely, if the laser is focused to a spot size smaller than the matched size, the normalized vector potential is so large that electrons near the axis will be blown out very rapidly while the electrons at the laser edge will feel a very small ponderomotive force so they move very little. This leads to a very wide sheath. In addition, the laser will diffract because its spot size is too small to be guided. To form a well-defined narrow sheath, which is a key assumption of our model, one needs the laser spot size to roughly be the same as the blowout radius, $W_0 \sim r_m$. Under this condition, electrons at an initial radius near W_0 will ex-

Downloaded 06 Jun 2006 to 198.11.27.24. Redistribution subject to AIP license or copyright, see http://pop.aip.org/pop/copyright.jsp

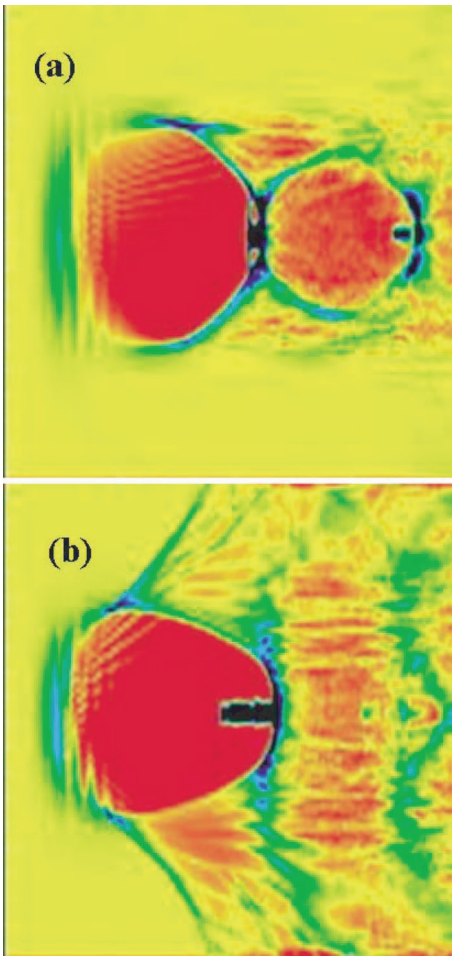

FIG. 5. (Color) Plasma density plots from PIC simulations with matched and unmatched spot sizes for the same laser power P and plasma density n_p, $P/P_c=8$ (a) matched case with $k_pW_0=4$ and $a_0=4$ (b) unmatched case with $k_pW_0=3$ and $a_0=5.3$ (the window size $[16c/\omega_p \times 16c/\omega_p]$ shown is only a fraction of the simulation box).

perience an impulse before the ion channel forces have fully developed. These electrons then move outward until the ion channel force brings them to rest. This suggests the blowout radius can be estimated by balancing the laser ponderomotive force on a single electron and the ion channel force. Typically, we also choose a laser pulse length around r_m, which is short enough that the impulse approximation is reasonable. Balancing the two forces to get an estimate of the matched spot size gives

$$\frac{a_0^2}{\bar{\gamma} k_p r_m} \sim k_p r_m, \tag{81}$$

and by substituting $\bar{\gamma} \sim a_0$, we get

$$k_p r_m \sim 2\sqrt{a_0}, \tag{82}$$

where the factor of 2 is deduced from full PIC simulations. Estimating the blowout radius in this manner was also done in Refs. 14 and 15, where an estimate of a factor of 2 smaller is given. In addition, it is also how the requirement for electron cavitation was determined in Ref. 22.

The need to use a matched laser spot size is illustrated in Fig. 5, where the plasma density is plotted from simulations with matched and unmatched spot sizes for the same laser power and plasma density. In Fig. 5(a) $k_pW_0=4$, while in Fig. 5(b) $k_pW_0=3$.

Our simple sheath model only works well for the matched case [Fig. 5(a)], therefore for the other value of W_0 our model [Fig. 5(b)] does not work as well. From the formula for r_m, Eq. (82), we can see that the ultrarelativistic limit, $r_m \gtrsim 4$, can be reached when $a_0 \gtrsim 4$ and $W_0 \sim r_m \sim 2\sqrt{a_0}$. Reaching this limit requires a laser power $P=[a_0^2W_0^2/32]P_c \sim 8P_c$, where P_c is the critical power for relativistic self-focusing.[19] For current state-of-the-art lasers,[6,20] $15 \lesssim P \lesssim 100TW$, reaching the ultrarelativistic blowout (bubble) regime therefore requires the use of plasma densities between $2\times10^{19} \gtrsim n_p \gtrsim 2\times10^{18}$ cm^{-3}, respectively.

IX. SUMMARY

We have described a nonlinear, kinetic (nonfluid) theory for describing multidimensional plasma wave wakefields generated by relativistic electron beams or intense short lasers with matched spot sizes propagating in plasmas. These wakefields are generated when all electrons within a radius r_b are expelled leaving behind an ion channel. The expelled electrons form a narrow sheath. The theory permits the derivation of an equation of motion for an electron at the blowout radius. Integrating this equation directly for electron beam drivers provides accurate agreement with fully nonlinear particle-in-cell simulation results. For laser drivers, the maximum blowout radius is determined from force balance and the equation of motion can then be used to determine the shape of the ion channel behind the laser. We have examined the consequences of this equation in the limit that $r_b \ll c/\omega_p$ and when $r_b \gg c/\omega_p$. For the small r_b limit we show how linear fluid theory breaks down and how the logarithmic divergence in the linear Green's function saturates for small radii. For the large r_b limit we show that the trajectory for r_b maps out a circle. We also discuss the differences between lasers and electron beam drivers. For e-beam drivers the spot size is typically much less than c/ω_p and for typical parameters the maximum blowout radius is $\lesssim 2c/\omega_p$. On the other hand, for lasers a matched spot size is required, $k_pW_0 \approx 2\sqrt{a_0}$, and the maximum blowout radius is typically $\gtrsim 4$.

ACKNOWLEDGMENTS

This work was supported by the DOE under Grants Nos. DE-FG02-03ER54721, DE-FG03-92ER40727, and DE-FG03-92ER40745. The simulations were done at NERSC and on the UCLA Dawson cluster.

[1] A. I. Akhiezer and R. V. Polovin, Sov. Phys. JETP **30**, 915 (1956).
[2] J. M. Dawson, Phys. Rev. **113**, 383 (1959).
[3] T. Tajima and J. M. Dawson, Phys. Rev. Lett. **43**, 267 (1979).
[4] P. Chen, J. M. Dawson, R. W. Huff, and T. Katsouleas, Phys. Rev. Lett. **54**, 693 (1985); **55**, 1537 (1985).
[5] W. Lu, C. Huang, M. Zhou, W. B. Mori, and T. Katsouleas, Phys. Plasmas **12**, 063101 (2005), and references therein; W. Lu, Master's thesis, UCLA, 2004.
[6] S. P. D. Mangles, C. D. Murphy, Z. Najmudin *et al.*, Nature (London) **431**, 535 (2004); C. G. R. Geddes, Cs. Toth, J. van Tilborg *et al.*, *ibid.* **431**, 538 (2004); J. Faure, Y. Glinec, A. Pukhov *et al.*, *ibid.* **431**, 541 (2004).

Downloaded 06 Jun 2006 to 198.11.27.24. Redistribution subject to AIP license or copyright, see http://pop.aip.org/pop/copyright.jsp

[7]M. Hogan, C. D. Barnes, C. E. Clayton *et al.*, Phys. Rev. Lett. **95**, 054802 (2005).
[8]R. A. Fonseca *et al.*, *Lecture Notes in Computer Science* (Springer, Heidelberg, 2002), Vol. 2329, III-342.
[9]J. B. Rosenzweig, B. Breizman, T. Katsouleas, and J. J. Su, Phys. Rev. A **44**, R6189 (1991).
[10]A. Pukhov and J. Meyer-ter-vehn, Appl. Phys. B: Lasers Opt. **74**, 355 (2002).
[11]J. B. Rosenzweig, AIP Conf. Proc. **647**, 577 (2002).
[12]N. Barov and J. B. Rosenzweig, Phys. Rev. ST Accel. Beams **7**, 061301 (2004).
[13]K. V. Lotov, Phys. Rev. E **69**, 046405 (2004).
[14]I. Kostyukov and A. Pukhov, Phys. Plasmas **11**, 5256 (2004).
[15]S. Gordienko and A. Pukhov, Phys. Plasmas **12**, 043109 (2005).
[16]P. Sprangle, E. Esarey, and A. Ting, Phys. Rev. Lett. **64**, 2011 (1990).
[17]D. H. Whittum, Phys. Plasmas **4**, 1154 (1997).
[18]P. Mora and T. M. Antonsen, Jr., Phys. Plasmas **4**, 217 (1997).
[19]P. Sprangle, E. Esarey, J. Krall, and A. Ting, IEEE Trans. Plasma Sci. **15**, 145 (1987).
[20]F. S. Tsung, R. Narang, W. B. Mori, C. Joshi, R. A. Fonseca, and L. O. Silva, Phys. Rev. Lett. **93**, 185002 (2004).
[21]E. Esarey, P. Sprangle, J. Krall, and A. Ting, IEEE Trans. Plasma Sci. **24**, 145 (1996).
[22]G.-Z. Sun, E. Ott, Y. C. Lee, and P. Guzdar, Phys. Fluids **30**, 526 (1987).

Downloaded 06 Jun 2006 to 198.11.27.24. Redistribution subject to AIP license or copyright, see http://pop.aip.org/pop/copyright.jsp